Journal of Alloys and Compounds 495 (2010) 509–512

Contents lists available at ScienceDirect

Journal of Alloys and Compounds

journal homepage: www.elsevier.com/locate/jallcom

Characterization of nanosized spinel ferrite powders synthesized by coprecipitation and autocombustion method

Juan Carlos Aphesteguy[a], Silvia E. Jacobo[a,*], N.N. Schegoleva[b,c], G.V. Kurlyandskaya[d]

[a] LAFMACEL, Fac. de Ingeniería, UBA, Paseo Colón 850, C1063EHA Buenos Aires, Argentina
[b] Ural State University, Dept. Magnetism and Magnetic Nanomaterials, Lenin Ave, 51, 620083 Ekaterinburg, Russia
[c] Institute of Metal Physics UD RAS, Kovalevskaya , 18, 620041, Ekaterinburg, Russia
[d] Universidad del País Vasco UPV-EHU, Dept. Electricidad y Electronica, 48940 Leioa, Spain

ARTICLE INFO

Article history:
Received 8 July 2008
Accepted 7 October 2009
Available online 4 November 2009

Keywords:
Nanoparticles
Soft magnetic materials
Chemical synthesis
Magnetic measurements
X-ray diffraction

ABSTRACT

Magnetic nanoparticles of magnetite (Fe_3O_4) and NiCuZn-doped magnetite ($Ni_{0.35}Cu_{0.15}Zn_{0.5}Fe_2O_4$) were prepared by coprecipitation and by sol–gel combustion methods accordingly. The average size, *d*, of magnetite nanoparticles (*d* = 12 nm) and the NiCuZn ferrite nanoparticles ignited at about 250 °C (*d* = 30 nm) was estimated from X-ray diffraction patterns. The Mössbauer spectroscopy revealed the existence of the paramagnetic doublet in both samples. For magnetite, coercive force of about 400 Oe was found at 5 K. Likewise, the coercive field of the NiCuZn-doped magnetite nanoparticles decreases with Fe^{2+} substitution at low temperature (260 Oe). This behavior can be explained taking into account the fact that the magnetocrystalline anisotropy constant of Fe_3O_4 is higher than that of NiCuZn ferrite.

1. Introduction

The development of nanosized magnetic materials is a subject of considerable interest both for understanding their fundamental properties and new technological applications [1–3]. High electrical resistance and lower saturation magnetization are the characteristics of soft ferrites, which are not found in traditional soft ferromagnets like silicon steels or permalloys [2]. Modern data storage, microwave protection and biomedical applications require strict control over the morphology of the particles and a considerable reduction of their dimensions, down to the single domain and superparamagnetic size [3].

The cubic MFe_2O_4 or $MO{\cdot}Fe_2O_3$ spinels represent a well known and important class of iron oxides where oxygen forms an fcc close packing, and M^{2+} and Fe^{3+} occupy either tetrahedral or octahedral interstitial sites. By adjusting the chemical identity of M^{2+}, the magnetic configurations of MFe_2O_4 can be molecularly engineered to provide a wide range of magnetic properties. Depending on the chemical identity of M^{2+}, the densely packed solid state form MFe_2O_4 nanocrystalline materials can have either high magnetic permeability and electrical resistivity (for M representing one or the mix components from Ni, Zn, Cu, etc.) or half-metallicity (for M = Fe), being of interest for future high-performance electromagnetic and spintronic devices [4,5]. Nanoparticles with controlled sizes and properties can be synthesized by wet chemical techniques [6–9]. The aim of present work is to identify doping effects causing the change of morphology, structure and magnetic properties of the designed spinel nanomaterial.

2. Experimental

2.1. Synthesis of magnetite nanoparticles (Fe_3O_4)

The magnetic nanoparticles were synthesized at 0 °C by mixing a water solution of $FeCl_2{\cdot}4H_2O$ (1.0 M) and $FeCl_3{\cdot}6H_2O$ (1.5 M) which has been previously flushed with N_2. Once the reaction temperature is reached, add of an oxygen-free solution of KOH 3 M dropwise slowly. The resulting solution was stirred for 2 h. The products were filtered, washed with deionizer water and methanol several times and dried in vacuum oven at 50 °C for 24 h. Samples were conserved in a vacuum oven for electrical and magnetic measurements.

2.2. Synthesis of NiCuZn ferrite nanoparticles ($Ni_{0.35}Cu_{0.15}Zn_{0.5}Fe_2O_4$)

NiCuZn ferrite nanoparticles were synthesized by using the autocombustion method. Stoichiometric amounts of $Ni(NO_3)_2{\cdot}6H_2O$, $Cu(NO_3)_2{\cdot}3H_2O$, $Zn(CH_3COO)_2{\cdot}2H_2O$, $Fe(NO_3)_3{\cdot}9H_2O$ and citric acid ($C_6H_8O_7$) were dissolved in distilled water at room temperature. Immediately it was titrated quantitatively by concentrated ammonia solution (NH_3) until the solution was neutral or slightly alkaline (pH 7–8), heating moderate and magnetic agitation. The solution was slowly evaporated until a highly viscous gel was formed after start the autocombustion 5 h later. Precursors calcined at 250 °C were studied in this work.

* Corresponding author.
E-mail addresses: caphestegu@fi.uba.ar (J.C. Aphesteguy), sjacobo@fi.uba.ar (S.E. Jacobo), vlasova@imp.uran.ru (N.N. Schegoleva), galina@we.lc.ehu.es (G.V. Kurlyandskaya).

0925-8388/$ – see front matter © 2009 Elsevier B.V. All rights reserved.
doi:10.1016/j.jallcom.2009.10.037

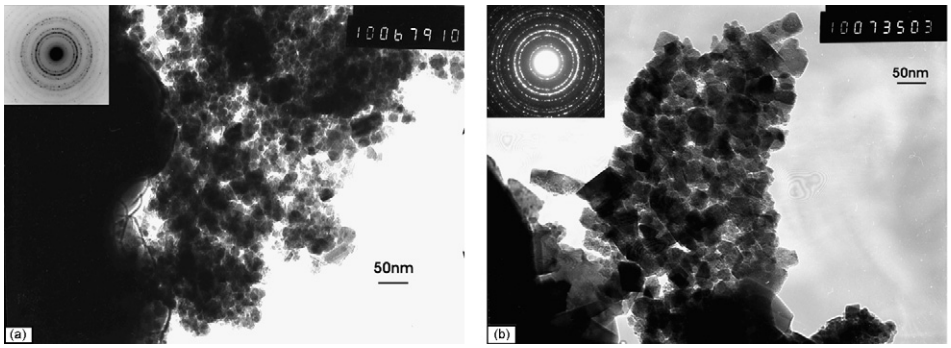

Fig. 1. Microphotographies (TEM) from magnetite (a) Fe_3O_4 and from $Ni_{0.35}Cu_{0.15}Zn_{0.5}Fe_2O_4$ (b).

Table 1
Measured lattice spacing *d* (Å), based on the rings in Fig. 1 and standard atomic spacing for (a) Fe_3O_4 and (b) NiCuZn ferrite along with their respective *h k l* indexes.

	Ring							
	1	2	3	4	5	6	7	8
(a) PDF: 19-0629								
d (Å)	4.85	2.96	2.52	2.18	1.71	1.60	1.51	1.47
Fe_3O_4	4.85	2.97	2.53	2.10	1.72	1.62	1.49	
h k l	111	220	311	400	422	511	440	620
(b) PDF: 48-0489								
d (Å)	4.85	2.98	2.54	2.42	2.10	1.72	1.62	1.48
$Cu_{0.1}Ni_{0.65}Zn_{0.65}Fe_{1.9}O_4$		3.01	2.56	2.45	2.12	1.72	1.63	1.49
h k l	111	220	311	222	400	422	511	440

2.3. Nanoparticle characterization

Nanoparticles were characterized by X-ray diffraction collected on a Rigaku model diffractometer equipped with a copper X-ray tube. Relative crystalline size was estimated for the integral intensity of the X-ray diffraction peak (3 1 1) by using Scherer equation. Transmission electron microscopy (TEM) was performed after sedimenting of the particles on carbon-coated copper grids. Mössbauer analysis has been done by ^{57}Fe Mössbauer spectroscopy at 298 K and isomer shifts values are reported with respect to metallic iron. Magnetic measurements were performed using a superconducting quantum interference device (SQUID) magnetometer (Quantum Design MPMS) at fields ranging from 0 to 10 kOe at the temperature rang of 5–300 K.

3. Results and discussion

X-ray diffraction patterns (not shown) indicate that samples are monophasic and that spinel phase is formed. The grain size calculated from XRD peak broadening using Scherrer's formula was 12 nm for magnetite and about 30 nm for NiCuZn ferrite.

TEM images (Fig. 1a and b) show that powders of both types consist of separate rather uniform from the point of view of their size slightly flattened nanoparticles. The selected area electron diffraction pattern (SAED) is shown in the onset of Fig. 1a and b for each system. The analysis of the distances pattern indicates that these materials are FCC spinels (Table 1). Magnetite particle size (Fig. 1a) ranges from 10 to 25 nm with an average size of about 14 nm. NiCuZn ferrite powder is significantly less uniform (Fig. 1b). Although it consists of the particles of the 15–40 nm, sometimes thin polycrystalline film areas were observed having the average of the crystallite size of about the same as for nanoparticles. The mean sizes for magnetite and NiCuZn ferrite are in reasonable agreement with the XRD results.

Mössbauer absorption spectra measured at room temperature for magnetite (a) and NiCuZn ferrite (b) nanoparticles are shown in Fig. 2. Spectra of both systems are fitted with two six-line subpatterns that are assigned to A-ions in tetrahedral sits and B-ions

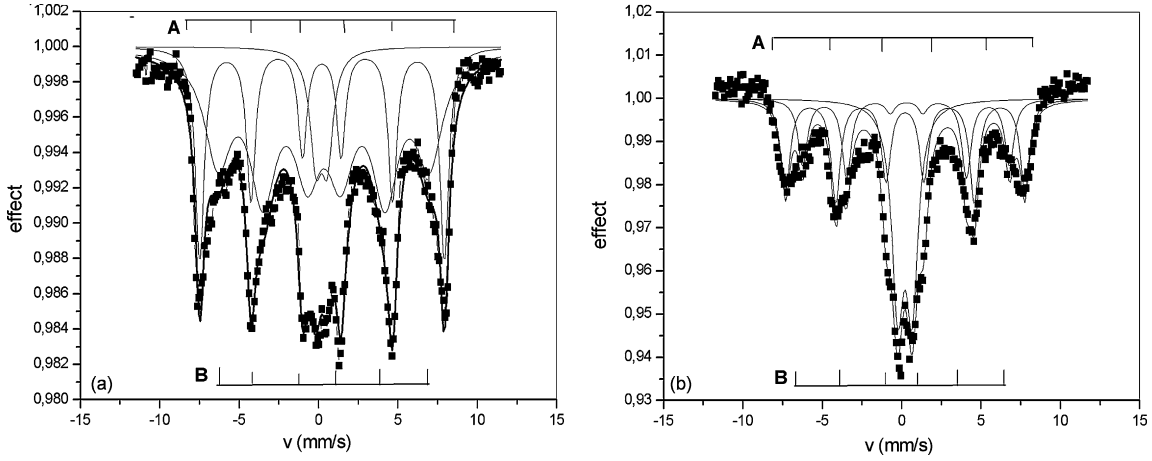

Fig. 2. Mössbauer spectra at RT of magnetite (a) and of NiCuZn ferrite (b) nanoparticles.

Table 2
Hyperfine parameters at RT for Fe_3O_4 and for NiCuZn ferrite.

Iron sites	Fe_3O_4				NiCuZn ferrite			
	Hyperfine field $\Delta H(T)$ (0.01)	Isomer shift δ (mm/s) (0.02)	Quadrupole splitting Δ (mm/s) (0.01)	%Fe	Hyperfine field $\Delta H(T)$ (0.01)	Isomer shift δ (mm/s) (0.02)	Quadrupole splitting Δ (mm/s) (0.01)	%Fe
Tetrahedral (A)	41.25	0.33	0.02	28.7	41.01	0.31	0.02	27.6
Octahedral (B)	47.73	0.45	0.03	62.9	46.88	0.38	0.06	47.4
Doublet	–	0.20	0.70	8.4	–	0.33	0.86	25

in octahedral sites of a typical spinel crystal structure and a large absorption of a doublet with very small magnetically split patterns. It is suggested that are paramagnetic and ferromagnetic contribution corresponding to both samples [10]. The difference between paramagnetic and ferromagnetic behavior can be explained by the superparamagnetic relaxation time τ, which is given by $\tau = \tau_0 \exp(KV/KT)$, where τ_0 is on the order of 10^{-9} to 10^{-12} and it depends only slightly on temperature (T), V is the volume of the particle, k is the Boltzman constant and K is the magnetic anisotropy constant. The sextet corresponds to the ferromagnetic particles of larger sizes as the time of magnetization vector relaxation (τ) is greater than the observation time (τ_{obs}), while the doublet is due to the smaller (superparamagnetic) particles for which $\tau_{obs} > \tau$ [11]. Superparamagnetic contribution (doublet) is larger in NiCuZn ferrite particles (25%) than in magnetite (8.4%). The broad size distribution, as shown in the TEM photograph (Fig. 1), is one reason why the samples have paramagnetic and ferromagnetic contributions at room temperature, simultaneously. In Fe_3O_4 spinel, four kinds of iron atoms, i.e. octahedral $Fe^{3+}$and Fe^{2+} and tetrahedral Fe^{3+} and Fe^{2+} coexist. However, fast electron exchange processes between the octahedral Fe^{3+} and Fe^{2+} at room temperature is expected to produce an average spectrum and is distinguished from that due to the tetrahedral sites. As it is seen from the Mössbauer values (Table 2), the observed Hyperfine Fields for the tetrahedral and octahedral sites in Fe_3O_4 spinel (47.73 and 41.25 T) are relatively lower than the reported values for spherical particles of 250 nm [12]. The isomer shift (δ) values, i.e. 0.33 and 0.45 mm/s for the tetrahedral and octahedral sites, respectively, indicate the presence of Fe^{3+} and Fe^{2+} ions in both sites. This shows that Fe_3O_4 spinel prepared by the present method is substantially inverted. It is well known that in NiZn ferrites Ni ions are preferably situated in octahedral [B] sites and Zn ions are preferably situated in the tetrahedral [A] sites. Also Cu ions prefer octahedral sites [10]. We have fitted the spectra based on a random distribution of Fe and Zn ions on the A sites. The smaller value of A-site isomer shift is due to a large covalency at the A-site and are consistent with the high spin Fe^{3+} charge states. Results for NiCuZn ferrite are in agreement reported by Kim et al. [10].

Field (H) dependence of DC magnetization (M) of magnetite (a) and of NiCuZn ferrite (b) at 300 and 5 K is shown in Fig. 3. It is well known that the saturation magnetization of a spinel ferrite largely depends on its composition and particle size, while the coercive field depends on composition, particle size and their shapes. The results indicate that the saturation magnetization for both systems increases continuously with magnetic field as they are samples with monodomain and superparamagnetic particles (8.4% and 25%) (Fig. 3). Due to the size of magnetite nanoparticles of >10 nm and of NiCuZn ferrite >30 nm and interacting system is observed and low values of coercivity are measured in both samples (onset of Fig. 3a and b).

Fig. 4 shows saturation magnetization (M_s at 10 kOe) and coercive field (H_c) at different temperature for both samples. Saturation magnetization for NiCuZn ferrite shows strong temperature dependence with fast decrease of the magnetization with temperature increase. One of the reasons of the observed temperature dependences is the presence of a significant fraction of superparamagnetic nanoparticles in NiCuZn ferrite. For both samples, the magnetization at room temperature is significantly less than that of the bulk magnetic particles (M_s for bulk magnetite is equal to 92 emu/g and M_s for bulk NiCuZn ferrite is equal to 73 emu/g [10]). The fact of the reduction of the saturation magnetization for magnetic nanoparticles comparing with their bulk properties is not something surprising: in general the smaller the particles are the higher this deviation is. The mechanisms of such a reduction are under development [11]. For example, the reduction of the saturation magnetization of about 30% was reported for very close to spherical 20 nm magnetite nanoparticles with low strains level [3]. The increasing coercivity values with decrease temperature for nanoparticles have been reported [12]. Coercivity depends from anisotropy constant (H_k) and saturation magnetization (M_s) ($H_c \propto H_k/M_s$). As H_k is higher in magnetite nanoparticles than in NiCuZn ferrite [13] and as H_k decays with temperature faster than

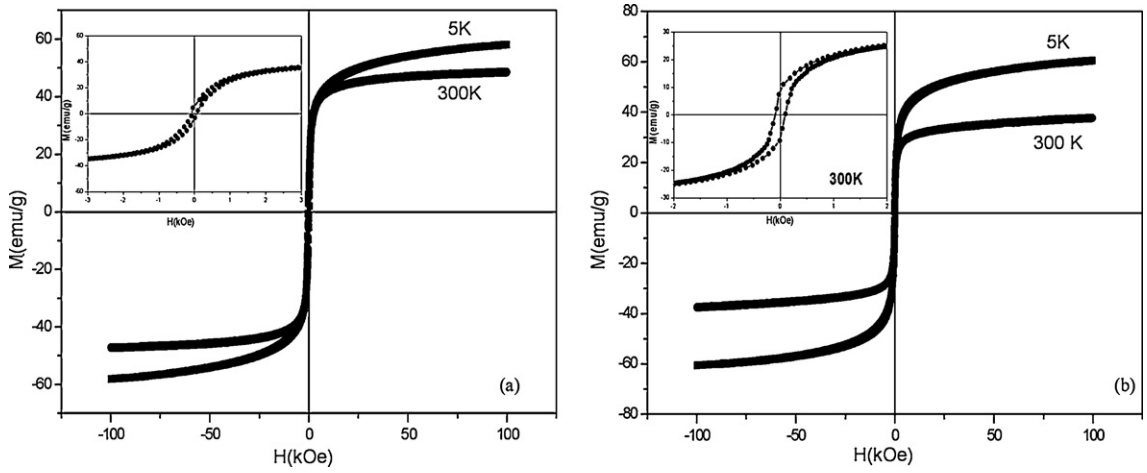

Fig. 3. Magnetization loops of magnetite (a) and of NiCuZn ferrite (b) nanoparticles at 300 K and at 5 K. Inset shows a detail at 300 K.

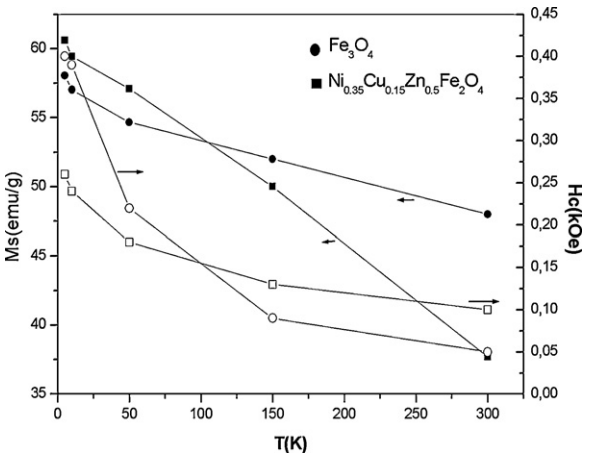

Fig. 4. Saturation magnetization (M_s at 10 kOe) and coercive field (H_c) for magnetite (Fe_3O_4) and of NiCuZn ferrite at 5, 50, 150 and 300 K.

M_S, H_c for magnetite increases abruptly at low temperature as Fig. 4 shows. Further studies are in progress.

4. Conclusions

In summary, Fe_3O_4 and NiCuZn ferrite nanoparticles have been successfully prepared by two wet chemical techniques. Both samples have been characterized showing single phase and nanosized particles with some superparamagnetic contribution. The saturation magnetizations at room temperature are significantly less than that of the bulk magnetic particles of both compositions Magnetite particles present more pronounced dependence of coercivity on temperature.

Acknowledgement

This work is supported by the University of Buenos Aires (grant I-055).

References

[1] L. Shu, S. Kao, Y. Liu, J. Wang, C. Jing, J. Zhang, J. Magn. Magn. Mater. 301 (2006) 100–106.
[2] S. Yan, J. Yin, E. Zhou, J. Alloys Compd. 450 (2008) 417–420.
[3] G.V. Kurlyandskaya, J. Cunanan, S.M. Bhagat, J.C. Aphesteguy, S.E. Jacobo, J. Phys. Chem. Solids 68 (2007) 1527–1532.
[4] G.V. Kurlyandskaya, S.M. Bhagat, C. Luna, M. Vazquez, J. Appl. Phys. 99 (104308) (2006) 1–5.
[5] T.A. Sorenson, S.A. Morton, G. Dan Waddill, J.A. Switzer, J. Am. Chem. Soc. 124 (2002) 7604–7609.
[6] A.S. Albuquerque, J.D. Ardisson, W.A.A. Macedo, et al., J. Appl. Phys. 87 (9) (2000) 4352–4357.
[7] A. Dias, R.L. Moreira, N.D.S. Mohallem, J. Phys. Chem. Solids 58 (4) (1997) 543–549.
[8] C.S. Kim, Y.S. Yi, K.T.P. Park, J. Appl. Phys. 85 (8) (1999) 5223–5225.
[9] L. Yu, S. Cao, Y. Liu, J. Wang, C. Jing, J. Zhang, J. Magn. Magn. Mater. 301 (2006) 100–106.
[10] W. Kim, S. Kim, S. Lee, Ch. Kim, J. Magn. Magn. Mater. 226–230 (2001) 1418–1420.
[11] K. Mandal, S.P. Mandal, P. Agudo, M. Pal, Appl. Surf. Sci. 182 (2001) 386–389.
[12] E. Schmidbauer, M. Keller, J. Magn. Magn. Mater. 297 (2006) 107–117.
[13] B.D. Cullity, Introduction to Magnetic Materials, Addison-Wesley Publishing Company, 1972, pp. 233–236.